

Yttria-stabilized zirconia thin films by pulsed laser deposition: Microstructural and compositional control

S. Heiroth^a, T. Lippert^{a,*}, A. Wokaun^a, M. Döbeli^b, J.L.M. Rupp^c,
B. Scherrer^c, L.J. Gauckler^c

^a Paul Scherrer Institut, General Energy Research Department, 5232 Villigen-PSI, Switzerland

^b Ion Beam Physics, Paul Scherrer Institut and ETH Zurich, 8093 Zurich, Switzerland

^c Nonmetallic Inorganic Materials, Department of Materials, Swiss Federal Institute of Technology, ETH Zurich, Wolfgang Pauli Str. 10, 8093 Zurich, Switzerland

Available online 7 July 2009

Abstract

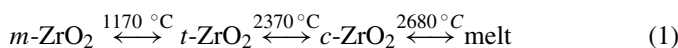
The ns-laser ablation characteristics of tetragonal 3YSZ versus cubic 8YSZ have been investigated to minimize a transfer of particulates in the pulsed laser deposition process. 3YSZ is significantly less prone to the exfoliation of μm -sized fragments than 8YSZ due to its enhanced fracture toughness, which allows the deposition of particulate-free films in a fluence range of $1.2\text{--}1.5\text{ J/cm}^2$. The influence of the PLD process parameters on the film microstructure and stoichiometry have been investigated with respect to the growth of dense 3YSZ layers with adequate adhesion to the *c*-cut sapphire single crystals. Dense 3YSZ films are obtained below a threshold pressure of ~ 0.025 mbar. At 600°C polycrystalline layers with a preferential (1 0 1) and (0 0 1) orientation and a columnar microstructure are formed while deposition at room temperature yields uniform amorphous layers. Strongly oxygen deficient films of the metastable t' phase are obtained at a low background pressure of 10^{-3} mbar. The meta phase films exhibit a low activation energy of 0.77 ± 0.02 eV and an enhanced d.c. electrical conductivity, e.g. 9×10^{-5} S/cm at 400°C , comparable or even higher than for 8YSZ films and bulk at temperatures up to 500°C .

© 2009 Elsevier Ltd. All rights reserved.

Keywords: YSZ; Films; Microstructure-final; Electrical conductivity; Fuel cells

1. Introduction

High temperature tetragonal and cubic zirconia phases (see Eq. (1)) are stabilized at room temperature by doping with soluble aliovalent oxides such as CaO, MgO, or Y_2O_3 . The doping introduces oxygen vacancies in the lattice, resulting in improved ionic conductivity at elevated temperatures.



The tetragonal-monoclinic transformation accompanied by a volume expansion of 3–5% may be triggered by external stress in partially stabilized zirconia (PSZ) opposing crack expansion in the material which results in excellent fracture toughness.¹ Fully stabilized, i.e. single phase cubic zirconia (FSZ) present at high dopant concentration, is attractive due to its enhanced ionic conductivity compared to the other phases.² Yttria-stabilized zir-

conia (YSZ) in particular exhibits a remarkable thermal stability, corrosion resistance, and interesting optical properties such as a high refractive index and low losses. A variety of thin film deposition techniques, i.e. spin coating,³ r.f. sputtering,⁴ pulsed laser deposition,^{5–7} chemical vapor deposition,⁸ and spray pyrolysis⁹ has been applied to deposit YSZ layers as high-*k* dielectrics in metal-oxide-semiconductor technology,^{5,10} optical or anti-wear coatings, buffer layers in superconductor thin film growth,⁴ and in miniaturized gas sensors and solid oxide fuel cells (SOFCs).¹¹ Reducing the electrolyte thickness to the sub- μm level is a key approach to minimize ohmic losses in SOFCs, which has recently been demonstrated to improve the cell performance significantly,¹² and allows for miniaturized micro-SOFCs.¹¹

Pulsed laser deposition (PLD) represents an effective technique for the thin film deposition of complex oxides. This is due to a prevalent congruent material transfer from the target to the film, its flexibility that enables a comprehensive microstructural control, and straightforward deposition of multilayer systems. A drawback frequently encountered in PLD is the transfer of droplets and particles.¹³

* Corresponding author. Tel.: +41 56 3104076; fax: +41 56 3102688.
E-mail address: thomas.lippert@psi.ch (T. Lippert).

This work aims at an elucidation of the laser ablation characteristics of *t*-3YSZ versus *c*-8YSZ and to investigate the influence of PLD process parameters on the film microstructure and composition particularly with regard to the deposition of dense, crack-free YSZ films with good adhesion to the substrate and of high ionic electrical conductivity. The electrical properties are analyzed and discussed with respect to the microstructure and stoichiometry of the films and their potential integration as electrolyte membranes in SOFCs. Due to the considerable reduction of the electrical resistance in sub- μm electrolyte membranes compared to conventional SOFC electrolytes (30–100 μm), even materials with slightly lower electrical bulk conductivity than state-of-the-art FSZ, like PSZ may be an eligible electrolyte material in thin film based SOFCs if they may provide advantages, e.g. in processing. To date, conductivity data for PSZ is scarce and limited to bulk ceramics samples.

2. Experimental

The YSZ thin films (450–550 nm) have been deposited by pulsed laser deposition on *c*-cut sapphire single crystals (10 mm \times 10 mm \times 0.5 mm) using a KrF or ArF excimer laser beam focused to a spot size of 2 mm² at a repetition rate of 10 Hz and 45° incident angle on the revolving target. The cylindrical targets were obtained by uniaxial pressing of 8 respectively 3 mol% Y₂O₃-doped ZrO₂ powder (Tosoh Corp., Japan) at 4.0 kbar and subsequent sintering for 10 h at 1600 °C respectively 4 h at 1400 °C. The substrates were mounted on a heatable rotary sample holder positioned at a fixed distance of 55 mm to the target. The applied substrate temperatures ranged from ambient temperature to 600 °C in an oxygen background (p_{O_2}) of 10⁻³–0.5 mbar which was adjusted after evacuation of the vacuum chamber to a base pressure of 2 \times 10⁻⁵ mbar. The optimum laser parameters in terms of wavelength and fluence were selected based on the ablation characteristics with regard to a minimization of particulates. The target morphology after an exposure to 100 pulses/spot and the ablated material collected on a substrate were analyzed by SEM for a range of fluences (0.7–5.3 J/cm²).

The microstructure of the PLD grown layers was investigated by scanning electron microscopy using a Zeiss Supra VP55 in variable pressure mode or prior sputtering of a 10 nm Pd layer to avoid charging. The crystallographic phase composition was analyzed on a Siemens D500 diffractometer with Bragg-Brentano geometry using Cu K α radiation. Raman spectra were acquired using a microscope setup (Witec, Germany) with a focal spot of \sim 300 nm diameter at an excitation wavelength of 442 nm and 15 mW output power of the He–Cd laser. The film roughness was measured using a Dektak 8 surface profiler. Thickness data derived from profilometry, Rutherford backscattering spectra and SEM cross-sectional images were consistent within \sim 10%.

Rutherford Backscattering Spectroscopy (RBS) and Particle Induced X-ray Emission (PIXE) using 2 MeV ⁴He ions respectively 3 MeV protons were applied as analytical tools to determine the chemical composition of the films.¹⁴

d.c. electrical resistivity measurements were conducted between 20 and 700 °C in air, N₂, H₂ and humidified H₂ atmospheres at a flow rate of 20 sccm for three temperature cycles at a rate of 3 °C/min in a tube furnace using a Keithley 2400 source meter. The thin films were measured in a two-point in-plane probe configuration. For this, two Pt-electrodes (0.5 mm \times 10 mm) of 5 mm spacing were sputtered on top of the film and contacted with Pt paste and wires. A ceramic glue was applied to fix the contacts.

Cylindrical polycrystalline bulk samples (\varnothing : 5 mm, length: 30 mm) fabricated analogously to the PLD targets and contacted with Pt paste and wires were investigated for comparison in a four-point probe configuration.

3. Results and discussion

3.1. Laser ablation characteristics

SEM micrographs of YSZ targets exposed to 100 pulses per spot reveal the formation of micro-cracks, which is most pronounced for low fluences \sim 1 J/cm². In the case of the 8YSZ target (Fig. 1a) deep cracks appear which apparently cause the detachment of flake-like μm -sized fragments and a significant roughening of the surface. The tetragonal 3YSZ target exhibits consistently only shallow micro-cracks and a stronger coherence of the grains, yielding smoother surfaces with hardly any indication of flake detachment (Fig. 1b). A comparison of SEM

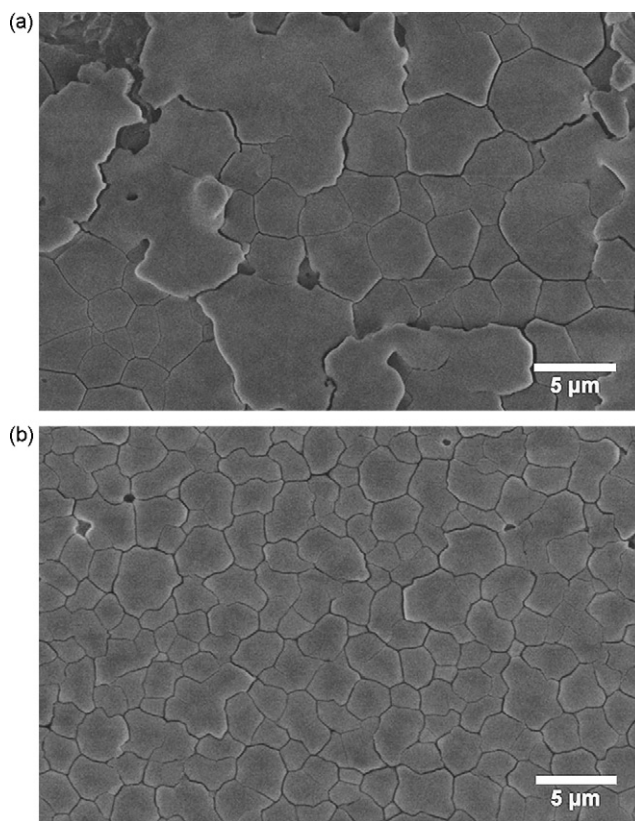


Fig. 1. Surface morphology of (a) a polycrystalline 8YSZ target and (b) a polycrystalline 3YSZ target after exposure to 100 laser pulses (λ : 193 nm, 0.75 J/cm²).

micrographs of PLD films grown under identical conditions from 3YSZ and 8YSZ targets (not shown) reveals a significantly lower areal density of incorporated μm -sized particles for 3YSZ at all fluences applied, which is in agreement with the analysis of the targets. Contrary to 8YSZ almost particulate-free 3YSZ films are obtained in a narrow fluence range of $\sim 1.2\text{--}1.5\text{ J/cm}^2$. At higher fluences spherical sub- μm droplets are detected in the films. A more detailed analysis of the ns-laser ablation characteristics of YSZ than this qualitative evaluation is beyond the scope of this paper. However, it should be mentioned that the excitation UV wavelength had no principal effect on the phenomena described beforehand, in agreement with results from Sanchez et al. for single crystalline YSZ.¹⁵

Cracking and subsequent fragmentation of the target in terms of exfoliation has previously been related to the thermal stress generated by rapid repetitive temperature jumps upon pulsed ns-laser irradiation.¹³ Similar to other refractory materials with a high thermal expansion coefficient and elastic modulus, e.g. tungsten and alumina, YSZ is prone to the expulsion of μm -sized particles of arbitrary shape after ns-laser irradiation. In the case of *t*-3YSZ the laser-induced stress may trigger a transformation to the monoclinic phase which hinders crack propagation due to the compressive strain generated by the associated volume expansion. An analogous process is not possible for the cubic phase which can explain the observed superior ablation characteristics of 3YSZ compared to 8YSZ. Therefore 3YSZ was used as the preferable target material in the subsequent PLD experiments to obtain YSZ films devoid of macroscopic defects. The ArF laser was employed at a fluence of 1.5 J/cm^2 since it provided a ~ 1.5 times higher deposition rate compared to the KrF laser.

3.2. Stoichiometry and phase composition of 3YSZ films

The chemical composition of the 3YSZ layers was analyzed by a combination of Rutherford Backscattering Spectroscopy (RBS) and Particle Induced X-ray Emission described in detail elsewhere.^{14,16} The film stoichiometries, normalized to the sum of cationic mole fractions, are $\text{Zr}_{0.93\pm 0.01}\text{Y}_{0.06\pm 0.01}\text{Hf}_{0.013\pm 0.001}\text{O}_{1.77\text{--}1.97\pm 0.04}$. Hafnium is detected as the only element in addition to Zr, Y and O, on a level of 1.6–2.0 wt.% which is common for zirconia-based compounds.¹⁷ The cations consistently yield stoichiometric ratios close to the values expected for a congruent transfer. The oxygen content however, depends clearly on the background pressure:

- Above ~ 0.05 mbar stoichiometric or only slightly oxygen deficient films with stoichiometry factors $x(\text{O}) = 1.96\text{--}1.97$ result.
- A strongly increasing oxygen deficiency reaching a stoichiometry factor as low as $x(\text{O}) = 1.77 \pm 0.04$ at 10^{-3} mbar is found for the low pressure domain

The observed pressure dependency can be interpreted in terms of the availability of oxygen background gas species as an additional source of oxygen in the film growth process. Light

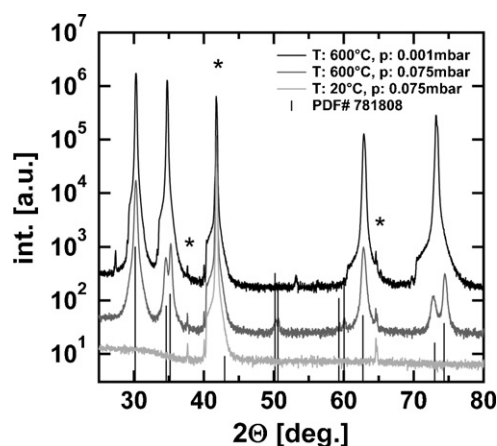


Fig. 2. X-ray diffraction patterns of 3YSZ films deposited at different substrate temperatures and oxygen background pressures on a logarithmic scale. Reflexes from the sapphire substrate are marked with an asterisk. The diffraction pattern of *t*-3YSZ powder as listed in the PDF-2 database of the International Centre for Diffraction Data (ICDD) is included as a reference. The abrupt rising edges of the most intense peaks are an artifact of the Ni filter used.

elements, such as oxygen, tend not to “stick” to the surface or they are preferentially sputtered from the growing film by arriving highly energetic species due to the absence of collisional moderation.

The effect of the PLD process parameters on the resulting crystallographic phase composition of the 3YSZ films is illustrated in Fig. 2 presenting exemplary X-ray diffraction patterns of three films deposited at different substrate temperatures and oxygen background pressures.

Layers deposited at room temperature exhibit irrespectively of the background pressure only reflexes originating from the sapphire substrate indicating their amorphous nature which is in agreement with previous reports for 8YSZ layers.^{7,16,18}

Polycrystalline films are obtained at a substantially higher substrate temperature of 600°C due to the enhanced surface mobility during the growth process. At background pressures above 10^{-2} mbar the diffraction patterns match the reference pattern for the tetragonal ZrO_2 phase with a characteristic doublet splitting of the $(X00)$ and $(00X)$ lines at $2\theta \sim 35^\circ$ and $72\text{--}75^\circ$. The axial ratio, c/a , of the pseudocubic lattice parameters decreases with the pressure to unity for the film deposited at 10^{-3} mbar, as shown in Fig. 3. The corresponding diffraction pattern consists only of singlet peaks and reveals a strong preferential (101) and (001) orientation. This pattern can be assigned to the metastable t'' phase ($P4_2/nmc$) with an axial ratio c/a of unity and alternate oxygen displacements along the c -axis¹⁹ or to the cubic ($Fm\bar{3}m$) fluorite structure.

X-ray diffraction provides no means to distinguish both phases owing to the small scattering factor of the oxygen atom and the resulting insensitivity to oxygen displacements. Raman spectroscopy as a probe to local bond distances and angles is particularly effective in the discrimination of zirconia polymorphs and allows a differentiation.^{19,20} The Raman spectrum of the layer deposited at 10^{-3} mbar shown in Fig. 4, reveals five characteristic bands at 255, 328, 470, 607 and 640 cm^{-1} which are indicative of a tetragonal phase confirming the formation of the

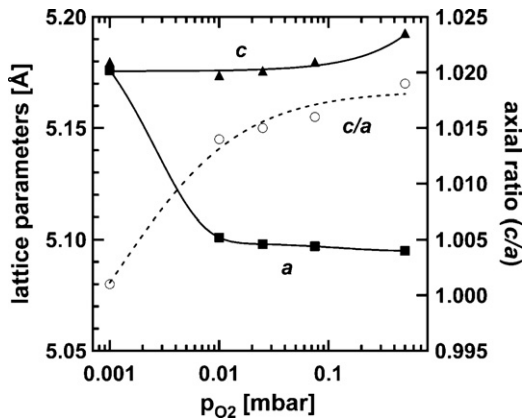


Fig. 3. Variation of the pseudocubic lattice parameters and the axial ratio, c/a , as a function of the oxygen background pressure applied for the deposition of crystalline 3YSZ films at 600 °C. Lines are included to guide the eye.

metastable t'' phase at low oxygen background pressure. The comparison of the reference spectra obtained on bulk YSZ samples indicates that the Raman spectrum of cubic zirconia on the other hand consists of a single broad peak at $\sim 617 \text{ cm}^{-1}$.

The t'' phase is stabilized by large dopant concentrations in ZrO_2 solid solutions and is normally detected for 7 and 9 mol% Y_2O_3 in yttria-stabilized zirconia.¹⁹ However, a shift of the tetragonal–cubic phase boundary to smaller dopant concentration has been noted for decreasing oxygen content in the system $\text{ZrO}_2\text{–CeO}_2$.²¹ The strong oxygen deficiency detected for films deposited in the low pressure regime may therefore be the origin of the t'' phase in layers containing just 3 mol% Y_2O_3 . Moreover, the non-equilibrium conditions in PLD, in particular the high kinetic energy of the ablated species at low background pressure favor the growth of metastable phases.²²

3.3. Microstructure of 3YSZ films

The dependency of the film microstructure on the applied substrate temperature and oxygen background pressure in the

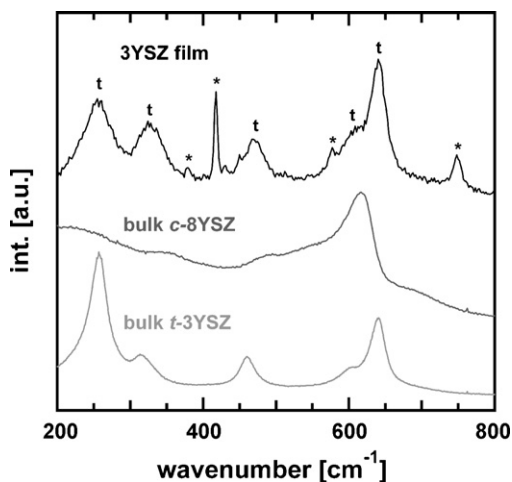


Fig. 4. Micro-Raman spectra of a crystalline 3YSZ film deposited at 600 °C, 10^{-3} mbar and, for comparison, of sintered bulk t -3YSZ and c -8YSZ samples. Raman bands of the sapphire substrate are marked with an asterisk, those indicative of a tetragonal phase with a t .

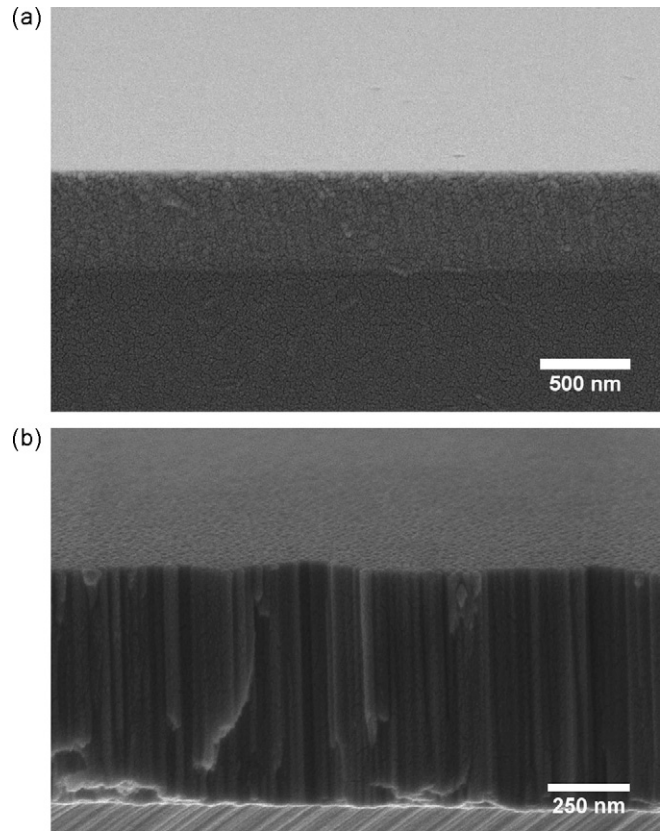


Fig. 5. Cross-sectional SEM images of 3YSZ films deposited at 0.01 mbar and a substrate temperature of (a) ambient temperature respectively (b) 600 °C. Tilt angle = 15°.

PLD process was investigated. Up to ~ 0.025 mbar, dense films with good adhesion to the substrate were obtained, which exhibit an isotropic, uniform microstructure in the case of amorphous layers (Fig. 5a) grown at room temperature, or, for crystalline films grown at 600 °C, a columnar microstructure (Fig. 5b). The mean column width increases with the pressure from ~ 10 nm (at 10^{-3} mbar) to ~ 20 nm (at 10^{-2} mbar) and to ~ 45 nm (at 0.025 mbar) together with the surface roughness rising from $R_q < 0.5$ nm at 10^{-3} mbar to 3.3 nm at 0.025 mbar, which is consistent with previous results.¹⁶ 3YSZ layers grown at higher pressures reveal an inferior adhesion to the substrate and an increasing porosity, especially in the case of amorphous layers (Fig. 6). As can be seen in Fig. 6, the structures are an assembly of spherical agglomerates with a diameter of typically 10–20 nm at 0.075 mbar which increases to 50–100 nm at 0.5 mbar. The spherical agglomerates probably originate from condensation in the plume since droplets from a molten target surface typically have a size of several hundred nm to micrometers.

The microstructural dependence on the deposition parameters, described above, agrees well with results published recently by Infortuna et al. on 8YSZ and Gd-doped ceria PLD films except that they obtained no amorphous films at ambient deposition temperature.²³ Dense fibrous columnar structures were observed below a threshold pressure of 0.05 mbar which is close to the value of 0.025 mbar found in this work.

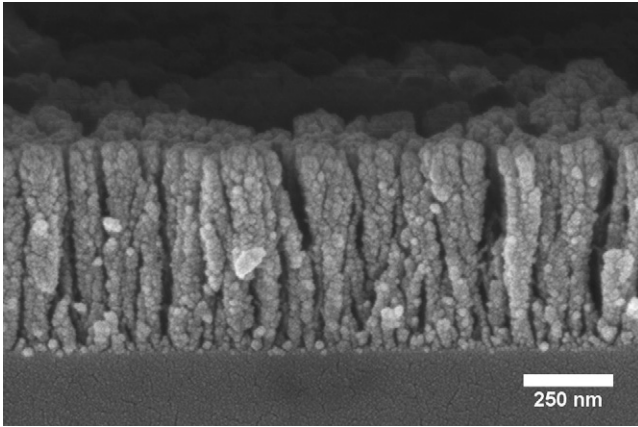


Fig. 6. Cross-sectional SEM image of an amorphous 3YSZ layer deposited at 20 °C and 0.075 mbar. The porous structure with large voids between columnar features is clearly visible. Tilt angle = 15°.

Di Fonzo et al. observed a transition from columnar structures to cluster assemblies with increasing pressure, p , and target to substrate distance, d , for alumina films grown on Si(100) substrates by PLD.²⁴ They proposed an empirical scaling law of $p^{0.5} \times d$ to predict a change from columnar dense to porous structures at 0.4 Pa^{0.5} m. Our experimental data of 0.34 Pa^{0.5} m for this transition suggests that this scaling law for microstructural growth characteristics is at least also valid for chemically similar systems.

3.4. Electrical conductivity of 3YSZ films

The electrical conductivity data of 3YSZ thin films are compared to bulk ceramic samples with grain sizes in the micron range (Fig. 7). Table 1 summarizes the conductivities of the investigated samples at selected temperatures of 400 and 600 °C as well as the derived activation energies and includes the respective oxygen stoichiometry factor. The conductivity of the t -3YSZ film deposited at 0.02 mbar and the bulk sample are similar, and as expected consistently lower compared to 8YSZ samples. The difference increases for higher temperatures due to the lower activation energies of 0.84 ± 0.02 eV for t -3YSZ films respectively 0.92 ± 0.01 eV for bulk t -3YSZ, compared to the ~ 1.1 eV commonly found for 8YSZ.^{3,6,16} To date, published conductivity data on 3YSZ is scarce and limited to bulk samples,²⁵ but shows a reasonable agreement to the results discussed above as Fig. 7 indicates.

The films deposited at 10^{-3} mbar which consist of the t'' phase, exhibit an enhanced electrical conductivity of e.g. $\sigma_{400^\circ\text{C}}$: $\sim 9 \times 10^{-5}$ S/cm as shown in Table 1. Comparable or even

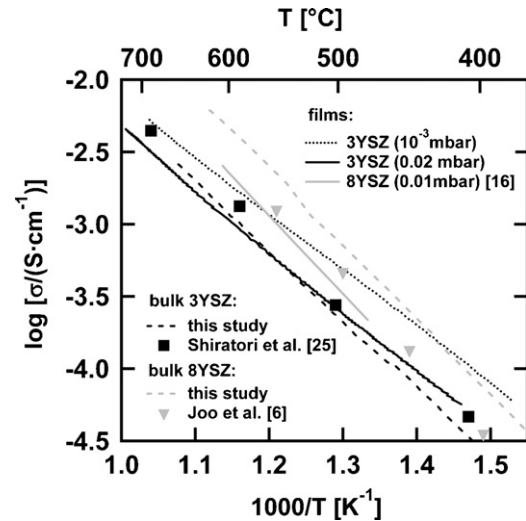


Fig. 7. Temperature-dependent d.c. electrical conductivity in air for bulk ceramic samples and crystalline YSZ films deposited at different oxygen background pressures and 600 °C.

higher conductivities than for 8YSZ bulk samples are obtained in the low temperature domain up to ~ 500 °C, due to the small activation energy of 0.77 ± 0.02 eV. These characteristics may originate from the pronounced oxygen deficiency in the t'' phase sample (compare Table 1) which yields a substantially increased concentration of oxygen vacancies as charge carriers in the film. Additionally, interfacial strain resulting from the lattice mismatch between film and substrate has recently been shown to enhance the ionic conductivity and lower the activation energy considerably in ultrathin, highly textured or heteroepitaxial YSZ layers.^{26,27} This effect is certainly relaxed by the granular growth and higher thickness of the films investigated here, but could still explain the lower activation energies compared to bulk samples, in particular for the t'' phase films which exhibit the strongest texture.

Fig. 8 depicts the measured temperature-dependent d.c. conductivity curves of the t'' phase film in different atmospheres. The reproducibility of the conductivity curves over multiple heating–cooling cycles is an indication that the t'' phase is stable over a large oxygen partial pressure range from air to hydrogen. A decrease of the conductivity and an increase of the activation energy from 0.77 ± 0.02 to 0.90 ± 0.02 eV is observed for a change from oxidizing to strongly reducing atmospheres. For an electronic contribution due to a potential reduction an increase of the total conductivity would be expected at low p_{O_2} which is not observed, therefore proving a predominantly ionic conduction. A decrease of the electrical conductivity at low p_{O_2} was

Table 1

Electrical conductivities at selected temperatures, activation energies and oxygen stoichiometry factors for the investigated YSZ films and bulk samples.

Sample	$\sigma_{600^\circ\text{C}}$ (mS/cm)	$\sigma_{400^\circ\text{C}}$ (mS/cm)	E_A (eV)	x (O)
3YSZ bulk	1.2	0.03	0.92	1.97
3YSZ film (T : 600 °C, p_{O_2} : 0.02 mbar)	1.1	0.04	0.84	1.90
3YSZ film (T : 600 °C, p_{O_2} : 10^{-3} mbar)	1.9	0.09	0.77	1.77
8YSZ bulk	4.9	0.07	1.04	1.92
8YSZ film (T : 600 °C, p_{O_2} : 0.01 mbar)	2.3	<0.03	1.08	1.91

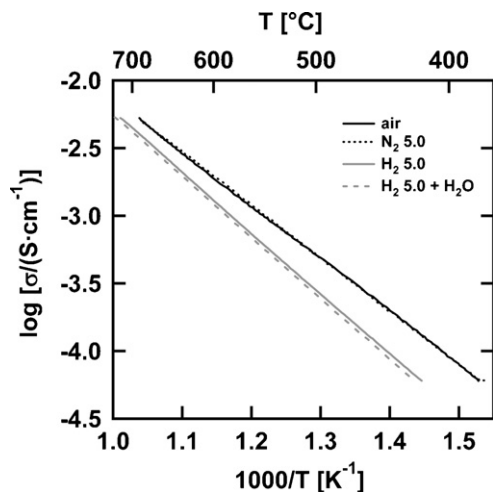


Fig. 8. Temperature-dependent d.c. electrical conductivity of a crystalline 3YSZ film deposited at p_{O_2} : 10^{-3} mbar and 600 °C (t' phase) in different atmospheres.

also observed by Kosacki et al. who postulated a change in the mechanism of charge carrier compensation, which reduces the charge carrier concentration.²⁸

Our data suggest that 3YSZ thin films can be applied as solid electrolyte membranes with an electrical performance comparable or even better than for 8YSZ in the low temperature range up to ~ 500 °C. The superior fracture toughness of the tetragonal 3YSZ could prove a particular asset to prevent thermal cracking²⁹ by the mismatch of thermal expansion coefficients of the different materials, which is typically encountered in SOFCs. However, the operational conditions must not allow for a spontaneous phase transition to the monoclinic phase.

4. Conclusions

The laser ablation characteristics of yttria-stabilized zirconia are characterized by an exfoliation of μm -sized fragments due to thermal cracking especially at low fluences while droplet ejection from the molten surface starts at fluences $> \sim 1.5$ J/cm². Tetragonal 3YSZ provides a superior fracture toughness due to the laser-induced martensite phase transformation enabling the deposition of practically particulate-free PLD thin films in a fluence range of 1.2–1.5 J/cm² contrary to cubic 8YSZ, where particulates are always observed. Microstructural analysis reveals that films of high density, as required in various fields of application, are only obtained below a threshold pressure of 0.025 mbar. At ambient temperature amorphous layers with an isotropic, uniform microstructure are formed. Polycrystalline 3YSZ films of the tetragonal phase with a preferential (101) and (001) orientation and a columnar microstructure form at a deposition temperature of 600 °C. The mean column width can be adjusted between ~ 10 and ~ 45 nm by variation of the pressure. At 10^{-3} mbar the metastable t' phase with an axial ratio c/a of unity is obtained. Its formation and stabilization are probably due to the observed substantial oxygen deficiency and the high kinetic energies of the plasma species arriving at the substrate at low p_{O_2} . The electrical conductivity is comparable or slightly higher than for 8YSZ in a temperature range up to 500 °C with a

reversible increase of the activation energy from 0.77 ± 0.02 eV in oxidizing to 0.90 ± 0.02 eV in strongly reducing atmospheres. The excellent additional mechanical characteristics of 3YSZ layers suggest a high potential for an application as solid electrolyte membranes in low temperature SOFCs.

Acknowledgements

The authors would like to thank Ruggero Frison for his assistance in preparing the ceramic targets. The project is part of the program 'Nanocrystalline ceramic thin films without sintering' (NANCER) funded by the Competence Center of Material Science and Technologies (CCMX) of the ETH board, Switzerland.

References

- Hannink, R. H. J., Kelly, P. M. and Muddle, B. C., Transformation toughening in zirconia-containing ceramics. *J Am Ceram Soc*, 2000, **83**, 461–487.
- Minh, N. Q., Ceramic fuel-cells. *J Am Ceram Soc*, 1993, **76**, 563–588.
- Chen, C. C., Nasrallah, M. M. and Anderson, H. U., Synthesis and characterization of YSZ thin-film electrolytes. *Solid State Ion*, 1994, **70**, 101–108.
- Rao, M. S. R., D'souza, C. P., Apte, P. R., Pinto, R., Gupta, L. C., Srinivas, S. and Bhatnagar, A. K., Microstructural study of yttria stabilized zirconia buffered sapphire for $\text{YBa}_2\text{Cu}_3\text{O}_{7-\delta}$ thin films. *J Appl Phys*, 1996, **79**, 940–946.
- Caricato, A. P., Di Cristoforo, A., Fernandez, M., Leggieri, G., Luches, A., Majni, G., Martino, M. and Mengucci, P., Pulsed excimer laser ablation deposition of YSZ and TiN/YSZ thin films on Si substrates. *Appl Surf Sci*, 2003, **208**, 615–619.
- Joo, J. H. and Choi, G. M., Electrical conductivity of YSZ film grown by pulsed laser deposition. *Solid State Ion*, 2006, **177**, 1053–1057.
- Zhu, J. and Liu, Z. G., Dielectric properties of YSZ high- k thin films fabricated at low temperature by pulsed laser deposition. *Mater Lett*, 2003, **57**, 4297–4301.
- Jiang, Y. Z., Song, H. Z., Gao, J. F. and Meng, G. Y., Formation and rate processes of Y_2O_3 stabilized ZrO_2 thin films from $\text{Zr}(\text{DPM})_4$ and $\text{Y}(\text{DPM})_3$ by cold-wall aerosol-assisted MOCVD. *J Electrochem Soc*, 2005, **152**, C498–C503.
- Perednis, D., Wilhelm, O., Pratsinis, S. E. and Gauckler, L. J., Morphology and deposition of thin yttria-stabilized zirconia films using spray pyrolysis. *Thin Solid Films*, 2005, **474**, 84–95.
- Zhu, J., Li, T. L., Pan, B., Zhou, L. and Liu, Z. G., Enhanced dielectric properties of ZrO_2 thin films prepared in nitrogen ambient by pulsed laser deposition. *J Phys D: Appl Phys*, 2003, **36**, 389–393.
- Bieberle-Hütter, A., Beckel, D., Infortuna, A., Muecke, U. P., Rupp, J. L. M., Gauckler, L. J., Rey-Mermet, S., Mural, P., Bieri, N. R., Hotz, N., Stutz, M. J., Poulidakos, D., Heeb, P., Müller, P., Bernard, A., Gmür, R. and Hocker, T., A micro-solid oxide fuel cell system as battery replacement. *J Power Sources*, 2008, **177**, 123–130.
- Shim, J. H., Chao, C. C., Huang, H. and Prinz, F. B., Atomic layer deposition of yttria-stabilized zirconia for solid oxide fuel cells. *Chem Mater*, 2007, **19**, 3850–3854.
- Chrisey, D. B. and Hubler, G. K., *Pulsed laser deposition of thin films*. John Wiley, New York, 1994.
- Döbeli, M., Characterization of oxide films by MeV ion beam techniques. *J Phys Condes Matter*, 2008, **20**, 7.
- Sanchez, F., Aguiar, R., Serra, P., Varela, M. and Morenza, J. L., Study of material emission in ArF and KrF excimer laser ablation of yttria stabilized zirconia single crystals. *Thin Solid Films*, 1998, **317**, 108–111.
- Heiroth, S., Lippert, T., Wokaun, A. and Döbeli, M., Microstructure and electrical conductivity of YSZ thin films prepared by pulsed laser deposition. *Appl Phys A: Mater Sci Process*, 2008, **93**(3), 639–643.

17. Stevens, R., *Zirconia and zirconia ceramics (2nd. ed.)*. Magnesium Elektron Ltd., 1986.
18. Mengucci, P., Barucca, G., Caricato, A. P., Di Cristoforo, A., Leggieri, G., Luches, A. and Majnia, G., Effects of annealing on the microstructure of yttria-stabilised zirconia thin films deposited by laser ablation. *Thin Solid Films*, 2005, **478**, 125–131.
19. Yashima, M., Kakihana, M. and Yoshimura, M., Metastable-stable phase diagrams in the zirconia-containing systems utilized in solid-oxide fuel cell application. *Solid State Ion*, 1996, **86–88**, 1131–1149.
20. Yashima, M., Ohtake, K., Kakihana, M., Arashi, H. and Yoshimura, M., Determination of tetragonal-cubic phase boundary of $Zr_{(1-x)}R_{(x)}O_{(2-x/2)}$ ($R = Nd, Sm, Y, Er$ and Yb) by Raman scattering. *J Phys Chem Solids*, 1996, **57**, 17–24.
21. Yashima, M., Morimoto, K., Ishizawa, N. and Yoshimura, M., Diffusionless tetragonal-cubic transformation temperature in zirconia-ceria solid solutions. *J Am Ceram Soc*, 1993, **76**, 2865–2868.
22. Bäuerle, D., *Laser processing and chemistry (3rd ed.)*. Springer, Berlin, 2000.
23. Infortuna, A., Harvey, A. S. and Gauckler, L. J., Microstructures of CGO and YSZ thin films by pulsed laser deposition. *Adv Funct Mater*, 2008, **18**, 127–135.
24. Di Fonzo, F., Tonini, D., Li Bassi, A., Casari, C. S., Beghi, M. G., Bottani, C. E., Gastaldi, D., Vena, P. and Contro, R., Growth regimes in pulsed laser deposition of aluminum oxide films. *Appl Phys A: Mater Sci Process*, 2008, **93**(3), 765–769.
25. Shiratori, Y., Tietz, F., Penkalla, H. J., He, J. Q. and Stöver, D., Influence of impurities on the conductivity of composites in the system $(3YSZ)_{1-x}-(MgO)_x$. *J Power Sources*, 2005, **148**, 32–42.
26. Garcia-Barriocanal, J., Rivera-Calzada, A., Varela, M., Sefrioui, Z., Iborra, E., Leon, C., Pennycook, S. J. and Santamaria, J., Colossal ionic conductivity at interfaces of epitaxial $ZrO_2:Y_2O_3/SrTiO_3$ heterostructures. *Science*, 2008, **321**, 676–680.
27. Kosacki, I., Rouleau, C. M., Becher, P. F., Bentley, J. and Lowndes, D. H., Nanoscale effects on the ionic conductivity in highly textured YSZ thin films. *Solid State Ion*, 2005, **176**, 1319–1326.
28. Kosacki, I., Suzuki, T., Petrovsky, V. and Anderson, H. U., Electrical conductivity of nanocrystalline ceria and zirconia thin films. *Solid State Ion*, 2000, **136**, 1225–1233.
29. Lei, C. H., Van Tendeloo, G., Siegert, M., Schubert, J. and Buchal, C., Structural investigation of the epitaxial yttria-stabilized zirconia films deposited on (001) silicon by laser ablation. *J Cryst Growth*, 2001, **222**, 558–564.